Multi-BVOC Super-Resolution Exploiting Compounds Inter-Connection

Antonio Giganti, Sara Mandelli, Paolo Bestagini, Marco Marcon, Stefano Tubaro
Dipartimento di Elettronica, Informazione e Bioingegneria - Politecnico di Milano - Milan, Italy
{antonio.giganti, sara.mandelli, paolo.bestagini, marco.marcon, stefano.tubaro}@polimi.it

***Abstract*—Biogenic Volatile Organic Compounds (BVOCs) emitted from the terrestrial ecosystem into the Earth's atmosphere are an important component of atmospheric chemistry. Due to the scarcity of measurement, a reliable enhancement of BVOCs emission maps can aid in providing denser data for atmospheric chemical, climate, and air quality models. In this work, we propose a strategy to super-resolve coarse BVOC emission maps by simultaneously exploiting the contributions of different compounds. To this purpose, we first accurately investigate the spatial inter-connections between several BVOC species. Then, we exploit the found similarities to build a Multi-Image Super-Resolution (MISR) system, in which a number of emission maps associated with diverse compounds are aggregated to boost Super-Resolution (SR) performance. We compare different configurations regarding the species and the number of joined BVOCs. Our experimental results show that incorporating BVOCs' relationship into the process can substantially improve the accuracy of the super-resolved maps. Interestingly, the best results are achieved when we aggregate the emission maps of strongly uncorrelated compounds. This peculiarity seems to confirm what was already guessed for other data-domains, i.e., joined uncorrelated information are more helpful than correlated ones to boost MISR performance. Nonetheless, the proposed work represents the first attempt in SR of BVOC emissions through the fusion of multiple different compounds.**

***Index Terms*—BVOC, Biogenic Emissions, Isoprene, Super-Resolution, Multi-Image Super-Resolution**

I. Introduction

Many chemicals are produced by terrestrial ecosystems, including volatile or semi-volatile compounds, and released into the atmosphere. Among all these chemicals, BVOCs have been recognized as significant contributors to air quality and climate change due to their large emission amount and high reactivity [1]–[4]. For instance, BVOCs are important precursors of ozone and secondary organic aerosols, which can negatively impact human health and vegetation growth [5], [6].

To assess air quality and climate conditions, it is crucial to accurately estimate the amount of BVOC emissions, both historically and in the present and future [2], [7], [8]. Although various ground-based techniques are available to sample BVOC emissions across different scales [6], [8], the available measurements are limited in space and time, making them less suitable for reliably simulating atmospheric, climate, and forecasting models.

To tackle the lack of measurements, we propose to increase the spatial resolution of BVOC emissions by refining a coarser grid. This problem falls into the general category of image SR tasks, which aim at enhancing the pixel resolution of a digital image. The goal is to find a suitable mapping between the Low Resolution (LR) image at hand and its corresponding High Resolution (HR) version in a way that ensures high-quality upscaling.

Plenty of work has been done to enhance classic 8-bit imagery like photographs or medical imaging. Several approaches have been proposed, and Deep Learning (DL)-based methods have shown to outperform classical methods [9] thanks to their ability to learn spatial features from huge datasets [10]. However, SR of 2D data linked to physical measures (like BVOC emissions) is less explored and not straightforward. Data involving physical acquisitions are always connected with a meaningful measurement unit; moreover, they might report a sparse nature, numerous outliers, and wide dynamic ranges. Therefore, the modification of standard SR techniques is usually required [11], [12].

The majority of the proposed works mainly exploit information coming from a single observation [12]–[16], i.e., the tackled problem can be formulated as a Single-Image Super-Resolution (SISR) task. Nonetheless, combining information from multiple different observations belonging to the same or similar domains proved a useful strategy to increase SR performance [17], [18]. This converts into a MISR task. For example, authors in [19] focused on improving the resolution of sea surface temperature by exploiting both optical and thermal images. A combination of information related to sea surface temperature, sea surface wind, and other remote-sensing products was proposed in [20] to reconstruct a denser ocean subsurface salinity. Authors of [21] exploited a pollution field's external factors and spatial-temporal dependencies to increase its resolution. In [22], SR of precipitation data was performed leveraging HR topography maps and various LR maps of sea level pressure and air temperature.

In this paper, we propose to fuse the emission maps of different BVOCs to provide denser emission maps. In particular, multiple LR emission maps are combined together and processed through a Neural Network (NN) to super-resolve emissions of a specific compound. To do so, we thoroughly explore the inter-connections between several BVOC species, investigating their structural similarities and spatial correlations. In our experiments, we compare various configurations regarding the species and number of aggregated compounds used for facing the proposed MISR objective. We show that a

This work was supported by the Italian Ministry of University and Research (MUR) and the European Union (EU) under the PON/REACT project.

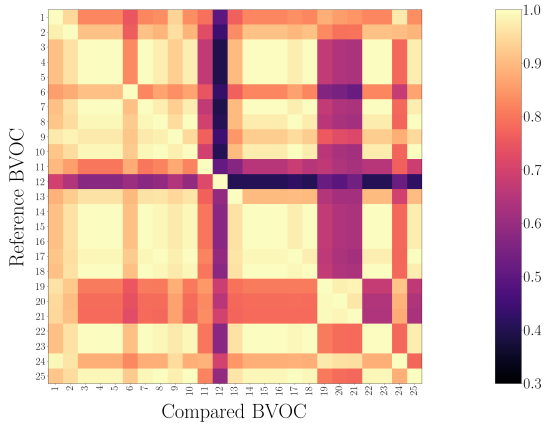

Fig. 1: Spatial inter-connection of multiple BVOC emission maps.

specific selection of BVOC species based on their related inter-connection can provide a performance gain in SR of emission maps. Interestingly, the aggregation of less correlated BVOCs proves more beneficial than the joint contribution of related compounds, similar to what was guessed in [19] for different domain data.

II. BVOCs Inter-Connection

The emissions related to different BVOCs are often inter-related, and changes in the emission rate of one compound can affect the emission rate of others. Several studies explored the complex underlying mechanism which governs these correlations [7], [23]. In principle, BVOC emissions strongly vary depending on the species of vegetation and on environmental, meteorological, and physiological factors. Moreover, environmental stress phenomena can induce other diving factors [24], [25].

In this section, we investigate the spatial inter-connection of BVOC emission maps related to multiple compounds. To do so, we select BVOC emission maps from the most recent global coverage biogenic emission inventory [26]. This inventory provides emissions from 25 different compounds, including isoprene, monoterpene, sesquiterpene, methanol, and other main BVOC species.

Given a reference biogenic compound, we explore its spatial inter-connection with other compounds by computing the Pearson Correlation Coefficient (PCC) and the Structural Similarity Index Measure (SSIM) between their emission maps. We always compare emission maps related to the same geographical area and acquisition date to obtain reasonable comparisons.

Fig. 1 depicts the computed inter-connection measures. Given the intrinsic commutative property of SSIM and PCC, the upper triangular region reports the SSIM, and the lower triangular region reports the PCC. The elements along the diagonal always equal 1 for both metrics, since the reference and the compared compounds are the same.

It is worth noticing that PCC and SSIM are in accordance one another, i.e., high PCC corresponds to high SSIM as well, and vice versa. Emission maps of different compounds actually contain some inter-correlations, i.e., the inter-connection matrix does not present a perfect diagonal behavior.

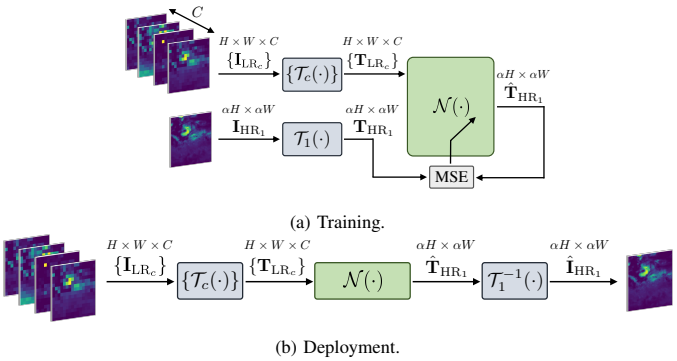

(a) Training.

(b) Deployment.

Fig. 2: The proposed Multi-BVOC Super-Resolution (MBSR) method: (a) training and (b) deployment phase.

These preliminary investigations motivate our proposed approach, that is, the joint exploitation of different BVOC emission maps for super-resolving LR maps. Following prior works in MISR over satellite-derived physical measures [19], [20], [22], we believe that the related cross-information among different compounds enables to boost performance with respect to the simple SISR scenario. In the next section, we present the proposed Multi-BVOC Super-Resolution (MBSR) strategy which is built upon this intuition.

III. Multi-BVOC Super Resolution

The proposed work for MBSR aims at exploiting spatial inter-connections between different BVOCs to super-resolve Low Resolution (LR) emissions. Differently from Single-Image Super-Resolution (SISR) tasks, we tackle a Multi-Image Super-Resolution (MISR) problem, in which a High Resolution (HR) emission map of a reference BVOC is recovered by exploiting multiple LR emission maps of different BVOCs.

Following the considerations done in Section II, we select C compounds according to their spatial inter-connections, stacking their emission maps in a set defined as $\{\mathbf{I}_{\mathrm{LR}_c}\}, c = 1, ..., C$. The set includes the reference BVOC LR emission $\mathbf{I}_{\mathrm{LR}1}$ associated with the index $c = 1$ and other joined compounds' LR emissions $\{\mathbf{I}_{\mathrm{LR}_c}\}, c = 2, ..., C$. The reference compound emission $\mathbf{I}_{\mathrm{LR}1}$ is the one we want to super-resolve. We propose to estimate an HR emission map as

$$\hat{\mathbf{I}}_{\mathrm{HR}_1} = \mathcal{T}_1^{-1}(\mathcal{N}(\{\mathcal{T}_c(\mathbf{I}_{\mathrm{LR}_c})\})), \tag{1}$$

where $\{\mathcal{T}_c(\cdot)\}$ collects C different data transformations $\mathcal{T}_c(\cdot)$, each one applied to the LR emission $\mathbf{I}_{\mathrm{LR}_c}$ of the c-th compound, $\mathcal{N}(\cdot)$ is a NN operator, and $\mathcal{T}_1^{-1}(\cdot)$ is the inverse transformation related to the reference BVOC, with $c = 1$.

Fig. 2 depicts a sketch of the proposed MBSR methodology. We model $\{\mathbf{I}_{\mathrm{LR}_c}\}$ and $\{\mathcal{T}_c(\mathbf{I}_{\mathrm{LR}_c})\}$ as tensors with size of $H \times W \times C$, where H and W represent height and width of the emission maps and C the number of compounds adopted for performing MBSR. Matrices $\mathbf{I}_{\mathrm{HR}_1}$ and its estimation $\hat{\mathbf{I}}_{\mathrm{HR}_1}$ have size $\alpha M \times \alpha N$, with $\alpha > 1$ indicating the super-resolution factor (i.e., how much we increase the resolution). The training phase involves $(\{\mathbf{I}_{\mathrm{LR}_c}\}, \mathbf{I}_{\mathrm{HR}_1})$ emissions as input (see Fig. 2a). At testing stage (see Fig. 2b), given a set of C LR emissions $\{\mathbf{I}_{\mathrm{LR}_c}\}$, we estimate $\hat{\mathbf{I}}_{\mathrm{HR}_1}$.

In our past investigations [12], we showed that a suitable data transformation is required to deal with BVOC emissions since they are characterized by sparsity, extremely small values, and wide dynamic ranges (from 10^{-30} to 10^{-9} [kg/m^{2}s]). As a matter of fact, BVOC emissions can present many outliers due to the large spatial diversity of the environmental factors driving the emission process, such as meteorology, type of vegetation, seasonal cycle, and atmospheric composition [12], [26]. For this reason, we adopt a set $\{\mathcal{T}_c(\cdot)\}$ of non-parametric transformations that force emission values to follow a uniform distribution between 0 and 1 [12], [27]. Notice that these transformations are compound-specific, i.e., every $\mathcal{T}_c(\cdot)$ strictly depends on the c-th compound since it is based on statistical information extracted from its emissions.

It is worth noticing that the choice of a NN as SR operator is not only motivated by the superior performances of novel DL-based methods with respect to classical approaches. In a MISR context, the advantage of solutions leveraging DL is that these do not require to discover a formal relationship between the different stacked BVOC emission maps. The training process benefits from any advantageous connections existing between multiple distinct types of input images [19]. In particular, we exploit the Second-order Attention Network (SAN) architecture [28], which can be considered the state-of-the-art in this field [12].

IV. Experimental Analysis

A. Dataset Collection

To perform our investigations, we use the most up-to-date and highest-resolution global coverage biogenic emission inventory available in the literature [26]. This inventory provides emissions from various BVOCs, covering the entire Earth's surface for the period of 2000-2020 at a high spatial resolution of $0.25°\times0.25°$, which is approximately 28km$\times28$km for each cell in continental regions.

As suggested in [12], we slice each emission map, which has a grid of 1440×720 cells, into non-overlapping patches of 64×64 cells. This step makes the computations more manageable and enables to assume minimal radial distortions due to the Earth's curvature. For every BVOC, we end up with 81957 distinct patches that we consider as HR references. The associated LR patches are generated by performing bicubic downsampling, resulting in 16×16 emission maps. Thus, we aim at super-resolving LR emission maps with $1° \times 1°$ spatial resolution into HR emission maps with $0.25° \times 0.25°$ resolution, which corresponds to a scale factor of $\alpha = 4$. We adopt this factor since it is more challenging with respect to smaller ones, as we found in our previous investigations [12].

Isoprene is the most prevalent and impactful BVOC in the inventory, accounting for approximately half of the total BVOC emissions [3]. Based on this, we focus on the SR of isoprene emission maps. To solve the MBSR task, we create $\{\mathbf{I}_{\mathrm{LR}_c}\}$ tensors by stacking one LR patch of isoprene and LR patches related to the same geographical area but to different BVOCs. Our final dataset is defined as $\mathcal{D} = \{\{\mathbf{I}_{\mathrm{LR}_c}\}_i, \mathbf{I}_{\mathrm{HR}_{1_i}}\}$, for $c = 1, ..., C$ and $i = 1, ..., 81957$. To select the joined compounds, we exploit the inter-connection metrics shown in Section II. In Section V, we provide more details on the selected compounds, comparing different experimental scenarios.

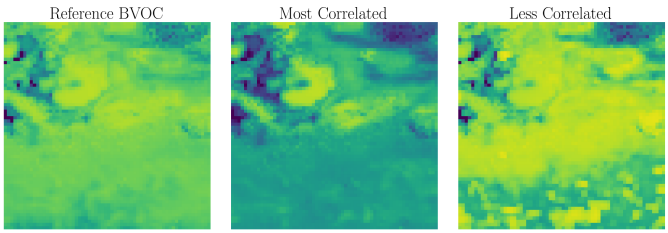

Fig. 3: Example of most correlated and uncorrelated BVOCs with respect to isoprene (reference BVOC).

B. Training Setup

As reported in [12], each compound needs a different data transformation based on statistical information derived from its HR emissions. To estimate the transformation set $\{\mathcal{T}_c(\cdot)\}, c = 1, ..., C$, we follow the experimental setup shown in [12].

We divide our dataset into train, validation, and test sets with $70/20/10$ percentage amount, respectively. We combine the ADAM optimizer with the Cosine Annealing learning rate scheduler [29], setting the initial learning rate to 10^{-4}, with a minimum value of 10^{-7}. We set a maximum number of $3 \cdot 10^5$ iterations, validating the model each 10^3 iterations and stopping the algorithm if the validation loss does not further improve after 10 validation steps.

V. Experimental Results

A. BVOC Inter-Connection Analysis

Our main goal is super-resolving isoprene emission maps, corresponding to index 11 in the BVOC inter-connection matrix shown in Fig. 1. Due to the substantial accordance between PCC and SSIM, we select the 3 most similar and the 3 least similar compounds based on their related SSIM.

From higher to lower, acetaldehyde, sesquiterpenes and, formaldehyde are the 3 best correlating compounds with isoprene. On the contrary, the 3 less correlated ones are MBO (2-methyl-3-buten-2-ol), methanol, and β-pinene. Fig. 3 shows an example of the spatial coherence between the reference compound (i.e., isoprene) and the most and least correlated compounds.

Vegetation emits all the selected compounds, and some are also partly products of the isoprene's oxidation in the atmosphere. In line with past works [23], [30], we found that the most inter-connected compounds are those influenced by similar environmental factors since similar plant species produce them. On the contrary, the compounds exhibiting a fairly low inter-connection are mainly produced by isoprene's oxidation [31]. We believe that these results are corroborated by the fact that oxidation phenomena are closely linked to atmospheric chemistry and meteorology, thus weakly related to geographic topology such as vegetation type.

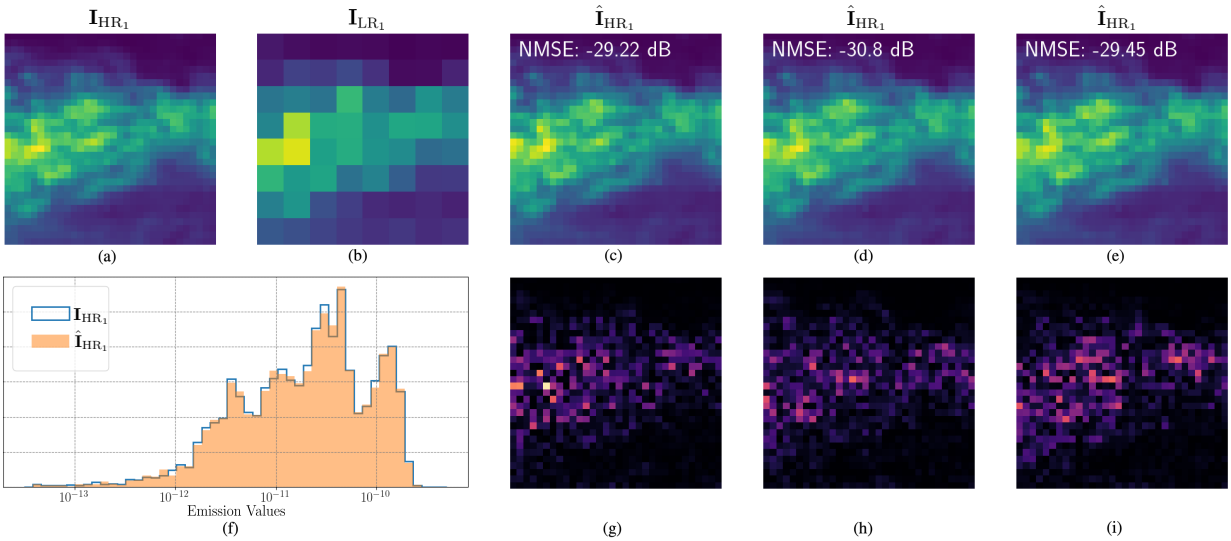

Fig. 4: Example of emission SR. (a) is the original HR isoprene emission map $\mathbf{I}_{\mathrm{HR}_1}$; (b) shows its related LR version $\mathbf{I}_{\mathrm{LR}_1}$; (c), (d), (e) are the SR emissions $\hat{\mathbf{I}}_{\mathrm{HR}_1}$ for the cases $C = 2$, $C = 3$ (best case) and $C = 4$, respectively; (g), (h), (i) their relative absolute error, computed as $|\mathbf{I}_{\mathrm{HR}_1} - \hat{\mathbf{I}}_{\mathrm{HR}_1}|$ (the brighter, the higher); (f) reports the histogram of the emission values of (a) ($\mathbf{I}_{\mathrm{HR}_1}$) compared with the best super-resolved emission map in (d), ($\hat{\mathbf{I}}_{\mathrm{HR}_1}$).

TABLE I: SR results for connected ($\mathcal{D}_{\mathrm{con}}$) and unconnected ($\mathcal{D}_{\mathrm{unc}}$) compounds. For $C = 2$, 1st and 2nd configurations denote the pairs (isoprene, acetaldehyde) and (isoprene, sesquiterpene) for $\mathcal{D}_{\mathrm{con}}$, and the pairs (isoprene, MBO) and (isoprene, methanol) for $\mathcal{D}_{\mathrm{unc}}$, respectively. In bold, the best achieved results.

Dataset		$C = 2$ SSIM / NMSE [dB]	$C = 3$ SSIM / NMSE [dB]	$C = 4$ SSIM / NMSE [dB]
$\mathcal{D}_{\mathrm{con}}$	1st	0.988 / −21.38	0.987 / −20.45	0.986 / −20.79
	2nd	0.986 / −20.92		
$\mathcal{D}_{\mathrm{unc}}$	1st	0.988 / −21.09	**0.989 / −21.93**	0.986 / −20.51
	2nd	0.987 / −21.31		

B. Compound Selection

In this section, we investigate how much leveraging the inter-connection between compounds benefits the SR process. To this purpose, we create different datasets based on the compound inter-connections, stacking multiple emission maps along the channel dimension of the tensors, as explained in IV-A. For brevity's sake, we reduce the potential compounds' combinations by selecting only strongly connected or poorly connected ones. The datasets of compounds that show a strong inter-connection with isoprene are generally denoted as $\mathcal{D}_{\mathrm{con}}$, while $\mathcal{D}_{\mathrm{unc}}$ indicates the datasets including less connected compounds.

For both $\mathcal{D}_{\mathrm{con}}$ and $\mathcal{D}_{\mathrm{unc}}$ categories, we consider the scenarios in which LR emission maps of $2, 3$, or 4 different compounds are aggregated to estimate HR emission maps of isoprene. For the case $C = 2$ (i.e., when 2 compounds are joined), we investigate two different configurations that correspond to joining isoprene with either acetaldehyde or sesquiterpenes in the $\mathcal{D}_{\mathrm{unc}}$ scenario, and to joining isoprene with either MBO or methanol in the $\mathcal{D}_{\mathrm{unc}}$ scenario. The case $C = 3$ aggregates to isoprene both acetaldehyde and sesquiterpenes in the $\mathcal{D}_{\mathrm{unc}}$ scenario and both MBO and methanol in the $\mathcal{D}_{\mathrm{unc}}$ scenario. Finally, $C = 4$ considers the 3 most correlating BVOCs for $\mathcal{D}_{\mathrm{con}}$ and the 3 least correlating BVOCs for $\mathcal{D}_{\mathrm{unc}}$.

Table I shows the achieved results in terms of average SSIM and Normalized Mean Squared Error (NMSE), where NMSE is defined as the MSE computed between $\mathbf{I}_{\mathrm{HR}_1}$ and $\hat{\mathbf{I}}_{\mathrm{HR}_1}$, normalized by the average of $\mathbf{I}^2_{\mathrm{HR}_1}$.

All configurations return good results. There are no remarkable differences between the configurations related to $C = 2$, i.e., there is not a specific compound which reveals more advantageous when paired with isoprene. On average, the configurations associated with $C = 4$ report the worst results. This might be due to some difficulties encountered by the training process in handling too many different data, thus compromising convergence. On the other hand, the proposed MBSR achieves a remarkable boost in using two additional uncorrelated compounds. In specific, SR benefits from information extracted from isoprene and the two mostly uncorrelated compounds, i.e., when $C = 3$, dataset $\mathcal{D}_{\mathrm{unc}}$.

We believe the spatial difference in the emission patterns favors extracting a distinctive feature by the NN, enabling to enhance the SR performance. Similar considerations were reported in [19], where the authors found that adding complementary information, even though less correlated with the data to be super-resolved, proved helpful for improving the SR results. Contrarily, the authors noticed that a positive correlation might result in redundancy which does not give an improvement in performance, and our achieved results seem to confirm this behaviour.

Fig. 4 shows examples of the proposed MBSR considering different configurations. In particular, we depict results for $\mathcal{D}_{\mathrm{unc}}$ in scenarios $C = 2, 3, 4$ (see Figs. 4c-e). To enhance the details, the emission maps correspond to cropped versions of the original emission patches. At the same time, NMSEs are referred to the entire images, to be comparable with the results in Table I.

It is worth noticing that the best configuration of Table I, i.e., $\mathcal{D}_{\mathrm{unc}}$ and $C = 3$, guarantees excellent results, especially in areas of high emission values. This can be seen

by comparing the absolute reconstruction errors associated with diverse configurations, computed as $|\mathbf{I}_{\mathrm{HR}_1} - \hat{\mathbf{I}}_{\mathrm{HR}_1}|$ (see Figs. 4g-i). In Figs. 4g and 4i, we can observe that higher deviations are reached at the areas with greater emission of the compound. This behavior is much more limited for the best configuration result shown in Fig. 4h. For a more detailed comparison, Fig. 4f compares the histograms of the ground-truth and of the estimated emission map through the best configuration, highlighting the significant reconstruction quality of the proposed methodology.

VI. Conclusions

In this paper, we proposed the Multi-BVOC Super-Resolution (MBSR) method, which combines multiple biogenic compounds to super-resolve coarse emission maps. To the best of our knowledge, there are no prior works investigating Multi-Image Super-Resolution (MISR) problems on BVOC. Nonetheless, SR of BVOC emissions is paramount to fill the lack of measurements for reliable atmospheric, climate, and forecasting models simulations.

To determine which and how many BVOCs should be combined, we conducted careful investigations on the spatial inter-connection between the most abundant BVOCs in nature. Then, we leveraged these inter-connections to drive the SR process. We experimented various configurations, aggregating the emission maps of different number of BVOCs with high and low spatial correlation. Interestingly, we found that joining poorly correlated compounds can effectively boost the SR performance, preserving spatial patterns and fine-scale structures.

Future works will concern the comparison of our proposed strategy with the state-of-the-art SR techniques for multispectral images, in which several related images are super-resolved simultaneously.

In addition, we will investigate the adoption of SR methods that embed known properties of the underlying physical system behind the SR process, and enforcing strict physical agreement and consistency [11] between LR and super-resolved data.

References

[1] B. Wang, Z. Li *et al.*, "Characteristics, secondary transformation potential and health risks of atmospheric volatile organic compounds in an industrial area in Zibo, East China," *Atmosphere*, vol. 14, 2023.

[2] A. B. Guenther, X. Jiang *et al.*, "The Model of Emissions of Gases and Aerosols from Nature version 2.1 (MEGAN2.1): an extended and updated framework for modeling biogenic emissions," *Geoscientific Model Development*, vol. 5, pp. 1471–1492, 2012.

[3] C. Calfapietra, S. Fares *et al.*, "Role of Biogenic Volatile Organic Compounds (BVOC) emitted by urban trees on ozone concentration in cities: A review," *Environmental Pollution*, vol. 183, pp. 71–80, 2013.

[4] J. Peñuelas and M. Staudt, "BVOCs and global change," *Trends in Plant Science*, vol. 15, pp. 133–144, 2010.

[5] A. Tani and T. Mochizuki, "Review: Exchanges of volatile organic compounds between terrestrial ecosystems and the atmosphere," *Journal of Agricultural Meteorology*, vol. 77, pp. 66–80, 2021.

[6] B. Opacka, J.-F. Müller *et al.*, "Global and regional impacts of land cover changes on isoprene emissions derived from spaceborne data and the MEGAN model," preprint, 2021.

[7] M. Cai, C. An, and C. Guy, "A scientometric analysis and review of biogenic volatile organic compound emissions: Research hotspots, new frontiers, and environmental implications," *Renewable and Sustainable Energy Reviews*, vol. 149, pp. 1–15, 2021.

[8] C. N. Hewitt, B. Langford *et al.*, "Quantification of VOC emission rates from the biosphere," *TrAC Trends in Analytical Chemistry*, vol. 30, pp. 937–944, 2011.

[9] X. Wang, J. Yi *et al.*, "A Review of Image Super-Resolution Approaches Based on Deep Learning and Applications in Remote Sensing," *Remote Sensing*, vol. 14, pp. 1–34, 2022.

[10] J. Baño Medina, R. Manzanas, and J. M. Gutiérrez, "Configuration and intercomparison of deep learning neural models for statistical downscaling," *Geoscientific Model Development*, vol. 13, pp. 2109–2124, 2020.

[11] A. Geiss, S. J. Silva, and J. C. Hardin, "Downscaling atmospheric chemistry simulations with physically consistent deep learning," *Geoscientific Model Development*, vol. 15, pp. 6677–6694, 2022.

[12] A. Giganti, S. Mandelli *et al.*, "Super-resolution of bvoc maps by adapting deep learning methods," *arXiv preprint arXiv:2302.07570v2*, 2023.

[13] R. Brecht, L. Bakels *et al.*, "Improving trajectory calculations by FLEXPART 10.4+ using deep learning inspired single image superresolution," *EGUsphere*, vol. 2022, pp. 1–17, 2022.

[14] B. M. Nguyen, G. Tian *et al.*, "Convolutional neural network modelling for modis land surface temperature super-resolution," in *European Signal Processing Conference (EUSIPCO)*, 2022.

[15] Y. Yasuda, R. Onishi *et al.*, "Super-resolution of near-surface temperature utilizing physical quantities for real-time prediction of urban micrometeorology," *Building and Environment*, vol. 209, pp. 1–15, 2022.

[16] K. Stengel, A. Glaws *et al.*, "Adversarial super-resolution of climatological wind and solar data," *Proceedings of the National Academy of Sciences*, vol. 117, pp. 16 805–16 815, 2020.

[17] T. Tarasiewicz, J. Nalepa, and M. Kawulok, "A graph neural network for multiple-image super-resolution," in *IEEE International Conference on Image Processing (ICIP)*, 2021.

[18] T. An, X. Zhang *et al.*, "Tr-misr: Multiimage super-resolution based on feature fusion with transformers," *IEEE Journal of Selected Topics in Applied Earth Observations and Remote Sensing*, vol. 15, pp. 1373–1388, 2022.

[19] D. T. Lloyd, A. Abela *et al.*, "Optically Enhanced Super-Resolution of Sea Surface Temperature Using Deep Learning," *IEEE Transactions on Geoscience and Remote Sensing (TGRS)*, vol. 60, pp. 1–14, 2022.

[20] T. Tian, L. Cheng *et al.*, "Reconstructing ocean subsurface salinity at high resolution using a machine learning approach," *Earth System Science Data*, vol. 14, pp. 5037–5060, 2022.

[21] N. Liu, R. Ma *et al.*, "Inferring fine-grained air pollution map via a spatiotemporal super-resolution scheme," in *UbiComp*, 2019.

[22] J. Wang, Z. Liu *et al.*, "Fast and accurate learned multiresolution dynamical downscaling for precipitation," *Geoscientific Model Development*, vol. 14, pp. 6355–6372, 2021.

[23] T. Stavrakou, J.-F. Müller *et al.*, "How consistent are top-down hydrocarbon emissions based on formaldehyde observations from GOME-2 and OMI?" *Atmospheric Chemistry and Physics*, vol. 15, pp. 11 861–11 884, 2015.

[24] J. Midzi, D. W. Jeffery *et al.*, "Stress-induced volatile emissions and signalling in inter-plant communication," *Plants*, vol. 11, 2022.

[25] J. Feldner, M. O. P. Ramacher *et al.*, "Analysis of the effect of abiotic stressors on BVOC emissions from urban green infrastructure in northern Germany," *Environmental Science: Atmospheres*, vol. 2, pp. 1132–1151, 2022.

[26] K. Sindelarova, J. Markova *et al.*, "High-resolution biogenic global emission inventory for the time period 2000–2019 for air quality modelling," *Earth System Science Data*, vol. 14, pp. 251–270, 2022.

[27] F. Pedregosa, G. Varoquaux *et al.*, "Scikit-learn: Machine learning in Python," *Journal of Machine Learning Research*, vol. 12, pp. 2825–2830, 2011.

[28] T. Dai, J. Cai *et al.*, "Second-Order Attention Network for Single Image Super-Resolution," in *IEEE Conference on Computer Vision and Pattern Recognition (CVPR)*, 2019.

[29] I. Loshchilov and F. Hutter, "SGDR: Stochastic gradient descent with warm restarts," in *International Conference on Learning Representations (ICLR)*, 2017.

[30] T. Karl, P. Harley *et al.*, "Efficient atmospheric cleansing of oxidized organic trace gases by vegetation," *Science*, vol. 330, pp. 816–819, 2010.

[31] G. M. Wolfe, J. Kaiser *et al.*, "Formaldehyde production from isoprene oxidation across no_x regimes," *Atmospheric Chemistry and Physics*, vol. 16, pp. 2597–2610, 2016.